Influence of slow synapses on the dynamics of neural models

François Rabelais Université
Physics Department

M.Arbabyazd

INSERM
Institut de neurobiologie de la méditerranée (Inmed)

Tutor:
Prof. Alessandro Torcini

Cotutor:
Dr. David Angulo

June 2016

1 Introduction

Complex dynamical systems are typically composed of many interacting units, these systems can be usually modelled in terms of sets of non-linear ordinary differential equations. Non-linear behaviour is ubiquitous in nature and ranges from fluid dynamics, via neural and cell dynamics to the dynamics of financial markets. Computational neuroscience is a recent theoretical/numerical discipline emerged in order to uncover the principles and mechanisms that guide the development, organization, information-processing and mental abilities of the nervous system.

Dynamical modelling of neural systems and brain functions has a history of success over the last half century. This includes, the Hodgkin-Huxley model. In 1952, A.L.Hodgkin and A.Huxley used the voltage clamp method to achieve the experimental data required to construct a mathematical model which describes the generation of action potentials in the neurons [23]. In 1963 they won the Nobel Prize in Physiology-Medicine for their contribution.

Epilepsy, a neurological disorder that affects millions of patients world-wide, arises from the concurrent action of multiple pathophysiological processes. Modern epilepsy research revealed short- and long-term alterations at several levels of neuronal organization in epilepsy. The power of mathematical analysis and computational modelling can be harvested to facilitate the understanding of the relative importance of such multifaceted, seizure-related changes taking place within highly non-linear and complex neuronal systems, with implications for both basic and clinical epilepsy research [4].

Recent evidence indicates that one of the possible causes of epilepsy and seizure generation is due to reorganization of neuronal tissue in the hippocampus, also known as reactive plasticity. In reactive plasticity, some neurons die whereas others, sprout and form novel aberrant connections. This phenomenon is best documented in the dentate gyrus of hippocampus, where granule cells axons (also known as mossy fibers) sprout to create new excitatory connections (through synapse) onto other cells. Thus, eventually there will be a novel recurrent excitatory network among mossy fiber region of hippocampus. Crépel et al. [18], reported that in the epileptic dentate gyrus, in addition to fast AMPA receptor synaptic currents ($\mathrm{EPSC_{AMPA}}$), slow Kainate receptor synaptic currents ($\mathrm{EPSC_{KA}}$) exists, while in healthy dentate gyrus there is no evidence of $\mathrm{EPSC_{KA}}$, implies that this novel excitatory connections are due to Kainate receptors.

Crépel et al. compared outgoing signals from AMPA receptor with Kainate receptor under two experiments, first stimulating a neuron with single-spike and second, stimulating it with periodic-spikes. From these experiments they observed a paradoxical behaviour in regularity of outgoing spikes; in first experiment, the generated spikes from AMPA receptor were completely precise and regular, while spikes from Kainate receptor were irregular [18]. However, in the second experiment they obtained contrary results, the Kainate receptor generated regular spikes, while AMPA receptor was responsible for irregular firing [8].

In this project we simulated this epileptic behaviour based on a mathematical model, called Integrate-and-fire model, and we obtained the same results for two experiments. From mathematical point of view, the inter-spike interval is the time difference of two adjacent successful spike firing, and its coefficient of variation (CV) is the criteria of its regularity. In single-spike simulation, as we expected the EPSCs from Kainate receptor was more irregular than EPSCs generated from AMPA receptor, while in periodic-spike simulation, on the contrary, Kainate receptor was responsible for regular firing, in confirm with experimental data [8].

This document is organized into five parts. Section 2 provides a general introduction to the elements of Neurophysiology needed to understand the experimental results. Section 3 focuses on foundations of computational neuroscience and its mathematical tools. It covers classic material such as the Hodgkin-Huxley model and the Integrate-and-fire model. Section 4 takes the simplified model derived in Part II

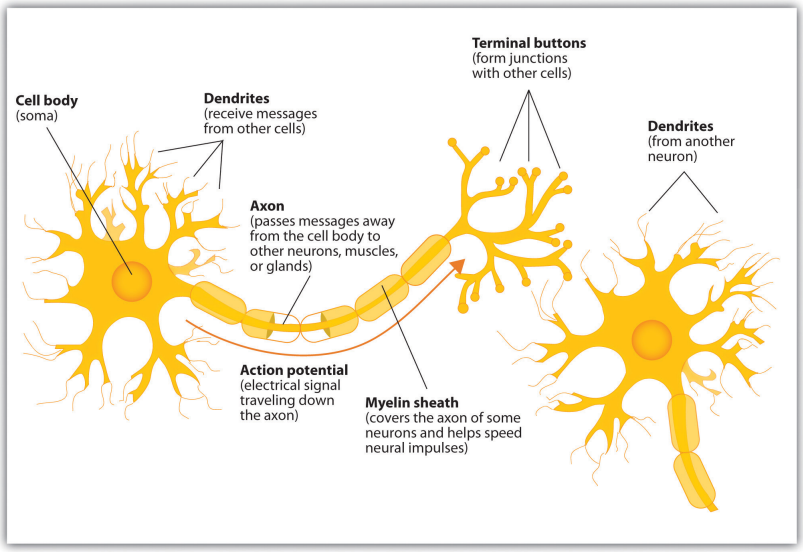

Figure 1: A typical neuron is divided into three main parts: the soma or cell body, dendrites, and axon. The dendrites receive incoming signals from adjacent neuron and then propagates them to the central processing unit of the neuron which is known as soma. The soma is the enlarged portion of a neuron that most closely resembles other cells. It contains the nucleus and other organelles and it coordinates the metabolic activity of the neurons. The axon is the main conducting unit of the neuron, capable of conveying electrical signals along distances that range from as short as 0.1 mm to as long as 2 m. The synapses are the junctions which connect the pre-synaptic terminal of one cell to the post-synaptic membrane of another cell.

and related mathematical backgrounds. In section 5, the experimental procedure and its results are well described. Finally, in section 6 the results of the simulation based on the experiment and analytical methods for interpreting the results are described.

2 Elements of Neurophysiology

The aim of this section is introducing some of the fundamental concepts of neurophysiology.
The elementary processing units in the central nervous system are neurons [20], which are of great importance because of their ability to transmit information in the brain [26]. They do this by generating firing sequences of characteristic electrical signals called action potentials or, more simply, spikes, in various temporal patterns; in general, neurons can not fire on their own, they do this as a result of incoming spikes as inputs from other neurons [15], through the connections called synapses which are treated in detail in the following sections.

2.1 Morphology

A typical neuron consists of three functionally distinct parts, called the dendrites, the soma, and the axon which are illustrated in Fig. 1.

The dendrites play the role of the "input device", which provides an enlarged surface area to receive signals from other neurons and transmits them to the soma. The shape of dendrites are of great importance because of their role in specialization of neurons; anatomically, there are four main types of neurons: unipolar in which dendrite and axon emerging from same process, bipolar in which have one axon and one dendritic

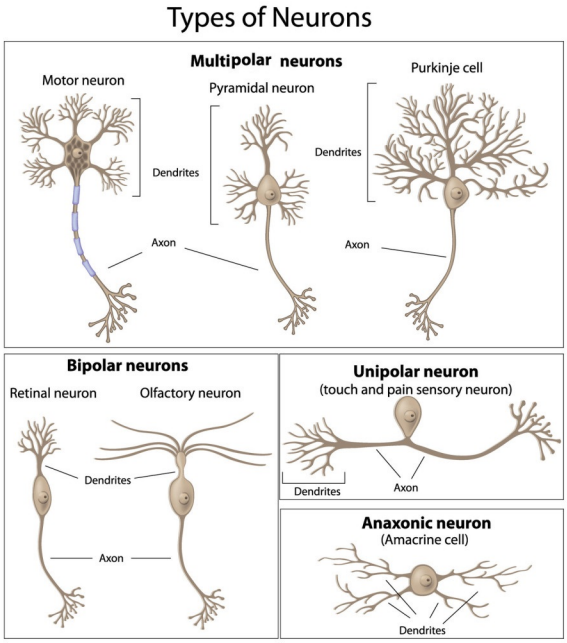

Figure 2: Four different types of neurons are shown. Their different shapes have important effects on neural processing. It has been proposed that despite their static structure, the dendrites are highly dynamic and appear to be capable of plastic changes during brain development, leading to modifications in branching pattern [38].

tree at opposing ends of the cell body, multipolar in which are composed of one axon and many dendritic trees, anaxonic where axon cannot be distinguished from dendrites, as shown in Fig. 2.

The soma is the "central processing unit" that performs integration of all the inputs coming from pre-synaptic neighbors [35].

The axons play the role of the "output device", which carry output and deliver the signal to other neurons. Axons terminate at sites called synapses, where the axon of a pre-synaptic neuron makes contact with the dendrite of a post-synaptic cell. Moreover, the elaborate branching structure of the dendritic tree allows neurons to receive the input from the neighbouring axon through these synaptic connections. Roughly speaking, there exists two types of synapses called chemical synapse, and electrical synapse (also called gap junction), see Fig. 3. However, the most common type of connection between neurons in the central nervous system of vertebrate brain is the chemical synapses [40], which will be described below.

The electrical synapse or gap junction is composed of two channel proteins called connexons which is a electrically conductive link between two neighbouring neuron; at gap junction, such cells approach within about 3.5 nm of each other [27]. These electrical connections are typically dendrite-to-dendrite or axon-to-axon [37]. Also there exists two types of electrical synapses, in the first type which is known as rectifying junctions, the ions can only flow one way, but the second type tend to be bi-directional and ions can generally flow both ways [11].

The chemical synapses are the principal mediators of targeted neuronal communication [37]. They pass information directionally from a pre-synaptic cell to a post-synaptic cell and are therefore asymmetric in structure and function. The gap between the post- and pre-synaptic terminals is larger than the gap junction (it is about 20nm wide [24]), and the mode of transmission is not electrical, but carried out by neurotrans-

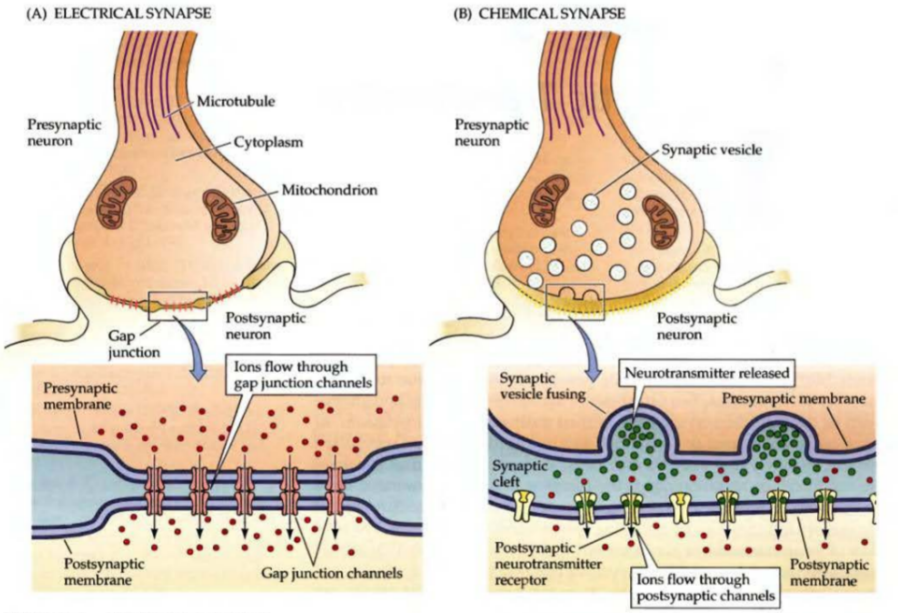

Figure 3: The electrical and chemical synapses differ fundamentally in their transmission mechanisms. In electrical synapses, the pores connect the two cells and ions from the pre-synaptic action potential diffuse directly into the post-synaptic neuron.The mechanism of chemical synapses is more complicated; when the action potential reaches the synapse, it triggers the release of vesicles which contain neurotransmitters and finally they will be received by specific receptors in the post-synaptic neuron.

mitters. These neurotransmitters are kept within small vesicles. At the arrival of an action potential at the axonal terminal, neurotransmitters are released into the synaptic cleft that is adjacent to another neuron.

These molecules then bind to receptors on the post-synaptic cell's side of the synaptic cleft. After binding, receptors allow the flow of different types of ionic currents. Depending on the nature of ions flowing into the post-synaptic cell, the chemical synapse can be either excitatory or inhibitory.

The shape of the pulse transmitted via chemical synapses can be modelled via the following equation, known as α-function [40]:

$$\Delta V_m = Ate^{-\alpha t} \tag{1}$$

Where ΔV_m denotes the difference between the membrane potential and the resting potential, A is for normalization which can also be considered as amplitude parameter, and α denotes the inverse of the post-synaptic time constant.

2.2 Physiology

Besides morphological features of neurons, they have physiological specializations [15].

The permeability of cell membranes to certain ions is achieved via ion channels that control the flow of ions across the cell membrane by opening and closing in response to voltage changes. There are different types of ion channels that can open and close under various conditions: Leakage channel, Voltage-gated ion channel, Ion pump, Ionotropic, Metabotropic(second messenger). Common ions involved in such processes within the nervous system are sodium (Na^+), potassium (K^+), calcium (Ca^{2+}), and chloride (Cl^-).

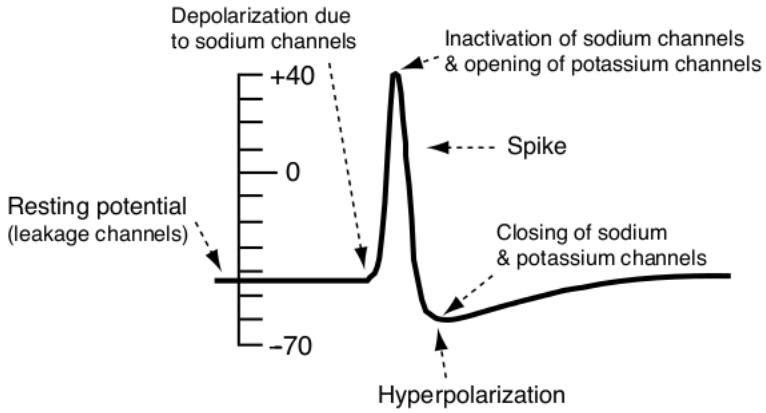

Figure 4: Typical form of an action potential. Spikes can be generated only if the incoming signals make the membrane potential more positive and reach the threshold.

The electrical potential difference between the interior of the cell and its surrounding is called the membrane potential. At rest, the cell membrane has a strongly negative polarization of about -65 mV. The voltage response of the post-synaptic neuron to a pre-synaptic spike is called the post-synaptic potential (PSP). If a post-synaptic neuron receives a sufficient number of spikes from several pre-synaptic neurons within a short time, its membrane potential becomes more depolarized, and if it reaches a critical value called threshold potential, then the neuron will generate an action potential. To go more into details of this mechanism, we introduce the excitatory post-synaptic potential or, more simply EPSP, and the inhibitory post-synaptic potential or IPSP, which depends on the nature of the ion flow into or out of the cell. If positively charged ion current flows into the cell and changes the membrane potential to less negative or even positive values, we call this process "depolarization"; while, if the positive current flows out of the cell, the membrane potential becomes more negative, a process which called "hyper-polarization", see Fig. 4.

Many different neurotransmitters have been identified in the nervous system. Common neurotransmitters include small organic molecules such as glutamate (Glu), gamma-aminobutyric acid (GABA), and dopamine (DA) [40]. Synaptic channels gated by the neurotransmitter Glu are a very common example of excitatory synapses with different types of receptors. One fast ionotropic Glu receptor is called -amino-3-hydroxy-5-methyl-4-isoxazolepropionic acid receptor, known as AMPAR. Another Glu receptor is called N-methyl-D-aspartate receptor, or simply NMDAR which is much slower and voltage dependent. A prominent example of inhibitory synapses uses the neurotransmitter GABA with a fast receptor called $GABA_\alpha$ and a slow receptor called $GABA_\beta$. The neurotransmitter DA has several receptor types, some of which are excitatory and some of which are inhibitory. It's worth to mention that abnormalities in the function of neurotransmitter systems contribute to a wide range of neurological and psychiatric disorders [31].

In the brain, or more precisely in the synapses, there are some chemical substances which by binding to a specific receptor, are able to activate or inactivate it. The term agonist refers to those chemicals that bind to a receptor and activates the receptor to produce a biological response. so agonist causes an action, while antagonist by binding to the related receptor, will block the action of the agonist.

In general there are five types of receptors: Glutamate, GABA, Acetylcholine, Dopamin, and Serotonin. The related receptors to the experiment is described below:
Glutamate receptors can be divided in two categories, ionotropic receptors and metabotropic receptors which are a G-protein coupled receptors (GPCR).

AMPA, Kainate, and NMDA considered in ionotropic category which are ligand-gated non-selective cation channels that allow the flow of K^+, Na^+ and Ca^{2+} in response to glutamate binding. Upon binding, the agonist will stimulate direct action of the central pore of the receptor, an ion channel, allowing ion flow and causing excitatory post-synaptic current (EPSC). This current is depolarizing and, if enough glutamate receptors are activated, may trigger an action potential in the post-synaptic neuron.
In Metabotropic category, GPCRs modulate synaptic transmission and post-synaptic excitability.
GABA receptors are a class of receptors that respond to the GABA which are gating anion channels that allow Cl^- ions to enter the post-synaptic neuron and causes hyper-polarization within the neuron, so they will decrease the probability of an action potential firing as the voltage becomes more negative.

2.3 Persistent Sodium Current

As it discussed in the previous section, the voltage-dependent activation and inactivation of sodium and potassium channels, leads to spike generation. Abnormal activity of Voltage-gated sodium channels (VGSCs) has long been linked to disorders of neuronal excitability such as epilepsy and chronic pain. Recent genetic studies have now expanded the role of sodium channels in health and disease, to include autism, migraine, multiple sclerosis, cancer as well as muscle and immune system disorders [16], and the role of VGSC blockers drugs in the treatment of these disorders [29]. As an example, Epilepsy is a disorder of neuronal excitability, characterised by episodes of excessive synchronised neuronal activity.

In this section we will introduce and compare two different types of sodium currents, known as transient sodium current (I_{NaT}) and persistent sodium current (I_{NaP}). Although inactivation is often referred to as a single process, there are at least two distinct kinetic classes of inactivation, termed fast and slow [3] [39].

The transient sodium current is the former type which at resting membrane potential, the sodium channel is closed requiring depolarization to be activated. Upon activation within a few hundred microseconds, they will depolarise the membrane potential further towards the equilibrium potential for sodium (+60mV in most neurons), resulting in an inward sodium ion current (Na^+), and finally within a few milliseconds they will inactivate which is considered as fast inactivation. The observations proposed that in many neurons, the fast inactivation process of Na^+ current is not complete and besides transient sodium current, the small percentage of slow inactivation current (typically less than 1% of the maximal transient current) which is referred to as persistent Na^+ current in the order of tens of seconds exists [14], and is open to serious questions [2].

The existence of I_{NaP} was first suggested by current clamp experiments in hippocampal [25], and it has been reported in a variety of cells: mammalian neurons located in neocortex, thalamus, entorhinal cortex, hippocampus, cerebellum, and squid axon [14]. In squid axon, the persistent sodium current activates at more negative potentials than the transient sodium current and hence has been called a “threshold” sodium current [21].

Despite its small amplitude compared with peak sodium current, I_{NaP} can alter firing behaviour profoundly, especially in the sub-threshold voltage range. I_{NaP} can be activated by small synaptic depolarizations and can then augment those potentials [36]. Clearly, an increase of only a few percent in the sodium current can dramatically alter cell firing and facilitate hyperexcitability, since it will amplify their responses to synaptic inputs (because it keeps the membrane depolarized longer), thereby driving them to repetitive firing [3], which in turn contributes to the chronic seizures [28]. The other consequences, including amplification of synaptic potentials and EPSP [34], generation of sub-threshold oscillations, heightened depolarization in the sub- and near-threshold voltage range, and reduced threshold for action potential firing [41].

Three general hypotheses about the origin of the non-inactivating current have been presented [14]. First, the window current hypothesis based on Hodgkin-Huxley whole cell current properties. But I_{NaP} probably is not due to a “window current”, reflecting overlap between the Hodgkin-Huxley activation and inactivation

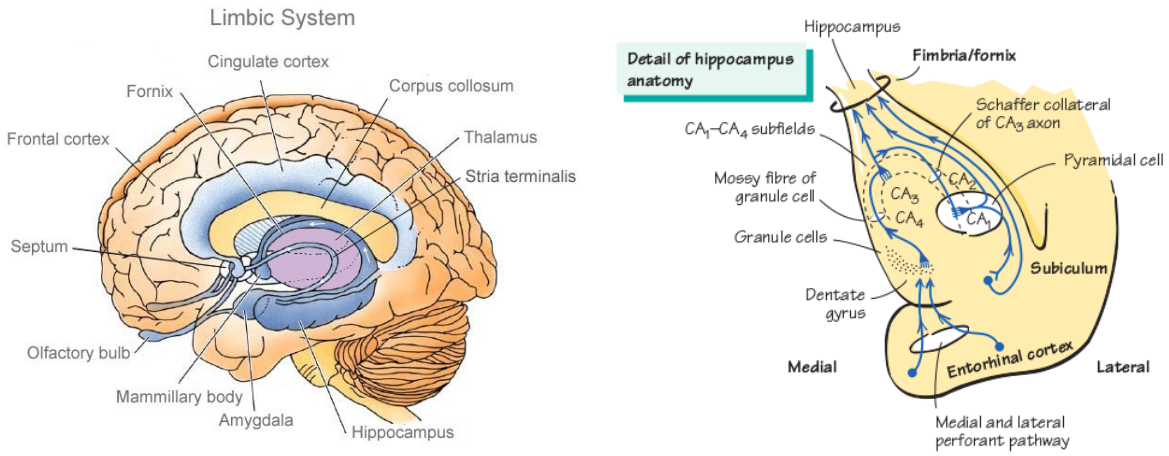

Figure 5: Location of Hippocampus in the brain and its components.

curves (i.e., a voltage range in which some channels are activated, while others are not yet inactivated) [36]. Besides this, the window current occurs only cover a restricted voltage range [41]. second, the possibility that I_{NaP} is generated by an unusual subtype of sodium channels that does not inactivate [19]; and third, recent evidence of a modal change in the inactivation properties of the transient sodium channels [3].

The calcium channel antagonist is cadmium, for the potassium channel is 3M CsCl, and for the sodium is Tetrodotoxin (TTX) [33]. In separate experiment French et al. group [19] blocked different channels and they realized the persistent current was blocked by TTX not other antagonists, so it was concluded that it was a sodium current. Also in their experiment they observed the persistent sodium current is activated in -60mV (about 10 mV negative to the transient sodium current [14]) which increased in amplitude with further depolarization to reach a maximum of -0.76nA at -40mV [19].

Goldin et al. have shown that slow inactivation does not depend on the fast inactivation gate, but one of the hypothesis is that it is due to the rearrangements of the channel pores [22].

2.4 Hippocampus

Hippocampus is a part of limbic system in Temporal lobe of brain and plays important roles in the consolidation of information from short-term memory to long-term memory and spatial navigation. Some of the brain diseases such as Alzheimer, Stress, Epilepsy, and Schizophrenia are related to this part of the brain. The hippocampus and its components are shown in Fig. 5.

In the hippocampus, granule cells of the dentate gyrus form distinctive unmyelinated axons that project along the mossy fiber pathway to the Cornu Ammonis area 3 (CA3). Granule cell synapses tend to be glutamatergic, but also evidence of GABAergic neurotransmitters within mossy fiber terminals has been detected. The signal a granule cell receives from a Mossy fiber depends on the function of the mossy fiber itself. Therefore, granule cells are able to integrate information from the different mossy fibers and generate new patterns of activity [7].

Dentate granule cells are thought to function in the formation of spatial memories [13]. Young and old dentate granule cells have distinct roles in memory function. Adult-born granule cells function in pattern separation whereas old granule cells contribute to rapid pattern completion [30].

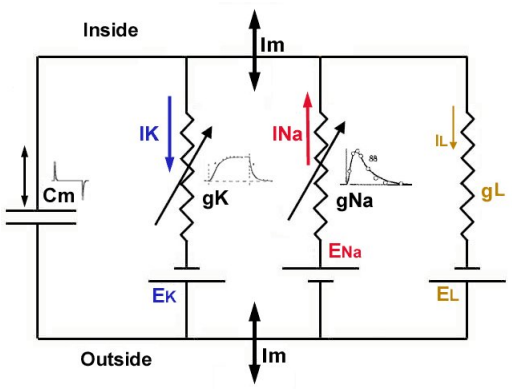

Figure 6: The Hodgkin-Huxley equivalent electrical circuit.

3 Mathematical Models

Biological neuron models aim to explain the mechanisms underlying the operation of the nervous system. In this section we will introduce two types of models for neuronal dynamics, the Hodgkin-Huxley model [23] and the Integrate-and-fire model [12].

3.1 The Hodgkin-Huxley Model

The HH model is a conductance-based models that describes the generation of action potentials in the neurons through a set of non-linear differential equations. Hodgkin and Huxley in 1952 used the voltage clamp method to achieve the experimental data required to construct mathematical descriptions of how the sodium, potassium and leakage currents depend on the membrane potential. In 1963 they received the Nobel prize in Physiology-Medicine for their contribution.

The equation for the membrane current is derived by summing up the various currents in the membrane, including Na^+, K^+, L which refers to a leakage current consists mainly of Cl^-; and also one external current [23]. By considering the interplay of these currents, if the external current is large enough, then a spike can be generated. See Fig. 7.

$$C_m \frac{dV}{dt} = -g_L(V - E_L) - g_{Na} m^3 h(V - E_{Na}) - g_K n^4 (V - E_K) + I \tag{2}$$

The circuit representation of the Hodgkin-Huxley model is illustrated in Fig. 6. This circuit includes a capacitor on which the membrane potential can be measured and three resistors with their own batteries, modelling the ion channels; two are voltage-dependent and one is static. The different gating variables are also described by differential equations, as follows:

Sodium activation gating variable:

$$\frac{dm}{dt} = \alpha_m(1 - m) - \beta_m m \qquad \alpha_m = 0.1 \frac{V + 40}{1 - \exp(-(V + 40)/10)} \qquad \beta_m = 4 \exp(-(V + 65)/18) \tag{3}$$

Sodium inactivation gating variable:

$$\frac{dh}{dt} = \alpha_h(1 - h) - \beta_h h \qquad \alpha_h = 0.07 \exp(-(V + 65)/20) \qquad \beta_h = \frac{1}{1 + \exp(-(V + 35)/10)} \tag{4}$$

$C_m = 1.0\mu Fcm^{-2}$		
I	E	g
Na^+	50 mV	120 $mScm^{-2}$
K^+	-77 mV	36 $mScm^{-2}$
L	-54.4 mV	0.3 $mScm^{-2}$

Table 1: Experimental data in Hodgkin-Huxley model.

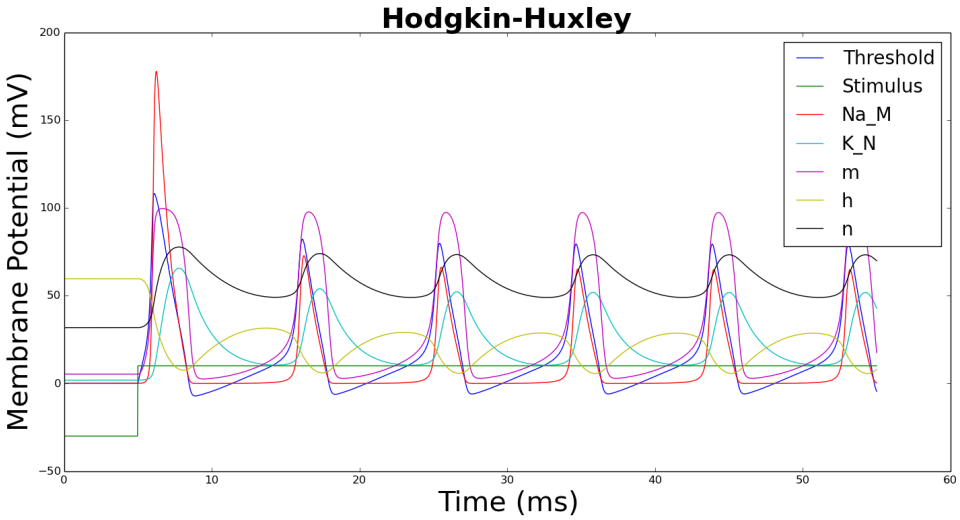

Figure 7: Simulation of spike generation in a neuron with Hodgkin-Huxley conductance-based model. If the external input causes the membrane voltage to rise, the conductance of sodium channels increases due to increasing m. As a result, positive sodium ions flow into the cell and raise the membrane potential even further. If this positive feedback is large enough, an action potential will be initiated.

Potassium activation gating variable:

$$\frac{dn}{dt} = \alpha_n(1-n) - \beta_n n \qquad \alpha_n = 0.01\frac{V+55}{1-\exp(-(V+55)/10)} \qquad \beta_n = 0.125\exp(-(V+65)/80) \tag{5}$$

3.2 The Integrate-and-Fire Model

The Integrate-and-fire (also known as IF) model is a common model of simplified neuron used in neural simulations. The IF model is comprised of a sub-threshold leaky-integrator dynamic, a firing threshold, and a reset mechanism. When the membrane potential reaches a certain threshold, a spike will be generated.

When the voltage is below the threshold θ, its value is determined by the equation for an RC circuit:

$$C_m\frac{dV}{dt} = -\frac{V-E_m}{R_m} + I \tag{6}$$

where C_m is the membrane capacitance, R_m is the membrane resistance and I is the total current flowing into the cell, which could come from an electrode or from other synapses.

we can also write this equation in terms of the membrane time constant τ_m, which is the product of C_m and R_m:

$$\tau_m \frac{dV}{dt} = -V + E_m + R_m I \tag{7}$$

When the membrane potential V reaches the threshold, the neuron fires a spike and the membrane potential V will reset to E_m. By solving above equation for V, the membrane potential increases from zero and follows an exponential time course, saturating at $R_m I$:

$$V = E_m + R_m I \left(1 - e^{\frac{-t}{\tau_m}}\right) \tag{8}$$

However, if $R_m I$ is bigger than the threshold θ, the voltage will cross the threshold at some point in time. The larger the current, the sooner this will happen. The membrane potential then resets to zero and the process repeats. For supra-threshold constant input, the integrate-and-fire neuron fires at a constant frequency.

In order to understand this equation better, we can analyse it and find the time when our system generates a spike. For a given level of current injection starting at time $t = 0$, at time T_{ISI} a spike occurs, when the membrane potential is equal to θ. By substituting $V = \theta$ and $t = T_{ISI}$ and rearranging the equation, the time to the spike T_{ISI} is:

$$T_{ISI} = -\tau_m \ln\left(1 - \frac{\theta}{R_m I}\right) \tag{9}$$

When a spike occurs and $R_m I$ exceeds θ, the argument of this logarithmic function is between zero and one. This makes the logarithm negative which, combined with the negative sign in front of τ_m, makes the time to the spike positive, as it should be. As the current increases, the $\frac{\theta}{R_m I}$ term gets smaller, and the argument of the logarithm approaches one, making the logarithm smaller. Thus the time to spike is shorter for greater input currents, as expected.

4 Theoretical Background

In this section we are going to introduce the mathematical backgrounds of our simulation on Experimental data.

4.1 Model

Our simulation was based on LIF model. The membrane potential $v(t)$ of the neuron evolves according to the following ordinary differential equation:

$$\dot{v}(t) = a - v(t) + gE(t), \qquad v(t) \in [-\infty, 1] \tag{10}$$

where all variables and parameters are now expressed in adimensional units. According to this equation, the membrane potential $v(t)$ evolves between minus infinity and one, and relaxes towards the value $a+gE(t)$.

When the membrane potential is equal to $v(t) = 1$, it means that it reaches the threshold value, then it will reset to $v(t) = 0$ and a spike is simultaneously sent to the post-synaptic neurons. This resetting procedure is an approximate way to describe the discharge mechanism operating in real neuron and results in a contribution to the coupling variable $E(t)$ [42].

The parameter $a > 1$ is the supra-threshold input DC current and g determines the strength and dependence of coupling on v and its sign determines whether the coupling is excitatory or inhibitory. The neural field $E(t)$ is the input synaptic current [1].

In order to describe accurately the post-synaptic response generated by the arrival of an action potential at a pre-synaptic terminal, there are two commonly used waveform equations as a synapse model [37],

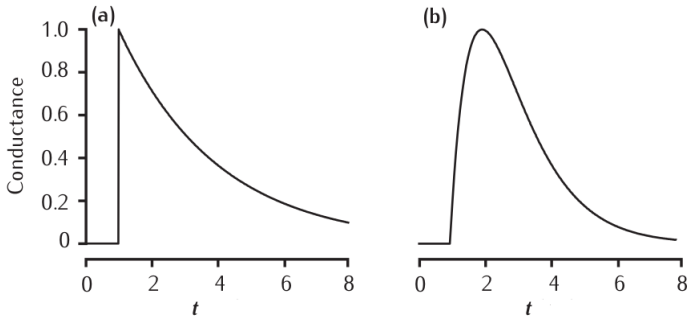

Figure 8: Two types of pulse shape: (a) single exponential decay with $\tau_\alpha = 3$, (b) dual exponential with $\tau_{\alpha_1} = 3$ and $\tau_{\alpha_2} = 1$.

called single exponential decay, and dual exponential function which are illustrated in Fig. 8, [32]. For an electrical response, the fundamental quantity to be modelled is the time course of the post-synaptic receptor conductance. The equations are:

$$F_1(t) = \alpha e^{-\alpha(t-t_0)} \tag{11}$$

$$F_2(t) = \frac{\alpha_1\alpha_2}{(\alpha_2 - \alpha_1)}[e^{-\alpha_1(t-t_0)} - e^{-\alpha_2(t-t_0)}] \tag{12}$$

which means if the membrane potential of the neuron reaches the threshold value ($v = 1$) at time t_0, then it will resets to zero and $E(t)$ will be incremented by these amounts ($F_i(t)$). The $\tau_\alpha = 1/\alpha$ here is corresponds to characteristic time scale of α-function.

The dual exponential waveform is more realistic representation of a typical synapse. We use this waveform when we want to consider the effects of rise and fall times in the coupling between neurons independently.

In the limit $\alpha_2 \to \alpha_1 = \alpha$, the dual exponential function will become like the following equation, known as α-function response:

$$F(t) = \alpha^2 t e^{-\alpha t}, t \equiv t - t_0 \tag{13}$$

which represents the shape of a single pulse emitted at time t by a neuron reaching the threshold value.

For this choice of the pulse shape, the field evolution is ruled by the following second order differential equation:

$$\ddot{E}(t) + 2\alpha\dot{E}(t) + \alpha^2 E(t) = \alpha^2 \tag{14}$$

Until now we see that the two equations (10) and (14) are responsible for the dynamics of our system. One of the methods to analyse this set of equations is by transforming the differential equations into a discrete-time event-driven map [10] and integrating from the time $t = t_n$, just after the deliver of the nth pulse, to time $t = t_{n+1}$, corresponding to the emission of the $(n+1)$th spike, thus it will reads as [6]:

$$E(n+1) = E(n)e^{-\alpha\tau(n)} + Q(n)\tau(n)e^{-\alpha\tau(n)} \tag{15}$$

$$P(n+1) = Q(n)e^{-\alpha\tau(n)} + \alpha^2 \tag{16}$$

$$v(n+1) = v(n)e^{-\tau(n)} + a(1 - e^{-\tau(n)}) + gH(n) \tag{17}$$

$$H(n) = \frac{e^{-\tau(n)} - e^{-\alpha\tau(n)}}{\alpha - 1}\left(E(n) + \frac{Q(n)}{\alpha - 1}\right) - \frac{\tau(n)e^{-\alpha\tau(n)}}{\alpha - 1}Q(n) \tag{18}$$

where $\tau(n) = t_{n+1} - t_n$ is the interspike time interval and for simplicity we introduced the auxiliary field $Q := \alpha E + \dot{E}$.

The interspike time interval $\tau(n)$ is associated with two successive neuronal firing, which can be determined by solving the following equation [5]:

$$\tau(n) = \ln[\frac{a - v_q(n)}{a + gH_q(n) - 1}] \tag{19}$$

here q identifies the neuron which will fire at time t_{n+1} by reaching the threshold value $v_q(\mathrm{n} + 1) = 1$.

The model so far introduced contains only adimensional units, however, the evolution equation for the membrane potential (10) can be easily re-expressed in terms of dimensional variables as follows:

$$\tau_m \dot{V}(\tilde{t}) = I - V(\tilde{t}) - \tau_m G\tilde{E}(\tilde{t}) \tag{20}$$

where we have chosen τ_m=10ms as the membrane time constant in agreement with the values reported in experiment [8]. Furthermore, $\tilde{t} = t.\tau_m$, the field $\tilde{E} = E/\tau_m$ has the dimensionality of frequency and G of voltage. The external excitatory current I have also the dimensionality of a voltage, since it includes the membrane resistance.

For the other parameters/variables the transformation to physical units is simply given by:

$$V = V_r + (V_{th} - V_r)v \tag{21}$$

$$I = V_r + (V_{th} - V_r)a \tag{22}$$

$$G = (V_{th} - V_r)g \tag{23}$$

where V_r = -60 mV, V_{th} = -50 mV.

4.2 Poisson Process

The description of the stochastic relationship between a stimulus (input) and a response (output) would require us to know the probabilities corresponding to every sequence of spikes that can be evoked by the stimulus. The probability that a spike occurs within the interval between times t and $t + \Delta t$ is proportional to the size of the interval, Δt, or more precisely $P(t) = \rho(t)\Delta t$, where $\rho(t)$ is called a probability density.

The firing rate $r(t)$ determines the probability of firing a single spike in a small interval around the time t, but $r(t)$ is not, in general, a sufficient information to predict the probabilities of spike sequences. For example, the probability of two spikes occurring together in a sequence is not necessarily equal to the product of the probabilities that they occur individually, because the presence of one spike may effect the occurrence of the other. If, however, the probability of generating an action potential is independent of the presence or timing of other spikes (i.e., if the spikes are statistically independent) the firing rate is all that is needed to compute the probabilities for all possible action potential sequences [15].

A stochastic process that generates a sequence of events, such as action potentials, is called a point process. In general, the probability of an event occurring at any given time could depend on the entire history of preceding events. If this dependence extends only to the immediately preceding event, so that the intervals between successive events are independent, the point process is called a renewal process. If there is no dependence at all on preceding events,or in other words, there is no memory of past events, so that the events themselves are statistically independent, we have a Poisson process. The Poisson process provides an extremely useful approximation of stochastic neuronal firing, and there are two case for it, the homogeneous Poisson process, for which the firing rate is constant over time, and the inhomogeneous Poisson process,

which involves a time-dependent firing rate.

The probability that an arbitrary sequence of exactly n spikes occurs within a trial of duration T, is given by $P_T(n)$ and is related to $P(t)$ with the following equation:

$$P(t) = n! P_T(n) (\frac{\Delta t}{T})^n \tag{24}$$

To compute $P_T(n)$, we divide the time T into M bins of size $\Delta t = \frac{T}{M}$. by taking the limit $\Delta t \to 0$, we assume that Δt is small enough so that we never get two spikes within any one bin.

$P_T(n)$ is the product of three factors: the probability of generating n spikes within a specific set of the M bins, the probability of generating spikes in the remaining $M - n$ bins, and a combinational factor equal to the number of ways of collocating n spikes into M bins. The probability of a spike occurring in one specific bin is $r\Delta t$, and the probability of n spikes appearing in n specific bins is $(r\Delta t)^n$. Similarly, the probability of not having a spike in a given bin is $(1 - r\Delta t)$, so the probability of having the remaining $M - n$ bins without any spikes is $(1 - r\Delta t)^{M-n}$. Finally, the number of ways of putting n spikes into M bins is given by the binomial coefficient $\frac{M!}{(M-n)!n!}$. Putting all together, finally:

$$P_T(n) = \lim_{\Delta t \to 0} \frac{M!}{(M-n)!n!} (r\Delta t)^n (1 - r\Delta t)^{M-n} \tag{25}$$

Since n is fixed, we can write $M - n \approx M = \frac{T}{\Delta t}$. by this approximation and defining $\epsilon = -r\Delta t$, we obtain:

$$\lim_{\Delta t \to 0} (1 - r\Delta t)^{M-n} = \lim_{\epsilon \to 0} ((1 + \epsilon)^{1/\epsilon})^{-rT} = e^{(-rT)} \tag{26}$$

For large M, $\frac{M!}{(M-n)!} \approx M^n = (\frac{T}{\Delta t})^n$, so

$$P_T(n) = \frac{(rT)^n}{n!} e^{(-rT)} \tag{27}$$

This is called the Poisson distribution.

If we use Stirling's formula in binomial equation, for large M we will have the Gaussian distribution:

$$P_G(n) = \frac{1}{\sigma\sqrt{2\pi}} e^{-\frac{(n - <n>)^2}{2\sigma^2}} \tag{28}$$

where $< n >$ is the mean, σ is the standard deviation of the inter-spike interval (ISI) and the coefficient of variation of ISI is $CV = \frac{\sigma}{<n>}$, which is a convenient measure of the variability of spike trains. For the binomial distribution as a general case we will have the following values:

$$< n >= rT \tag{29}$$

$$\sigma = \sqrt{rT(1 - rT/M)} \tag{30}$$

$$CV = \sqrt{\frac{1 - rT/M}{rT}} \tag{31}$$

It obvious that if we consider large value for M, which corresponds to large number of bins, then these equation will become simpler and the mean and the variance will be equal, $\sigma^2 =< n >= rT$. In Fig. 9 we demonstrate the transition from the Poisson distribution to Gaussian distribution by increasing rT.

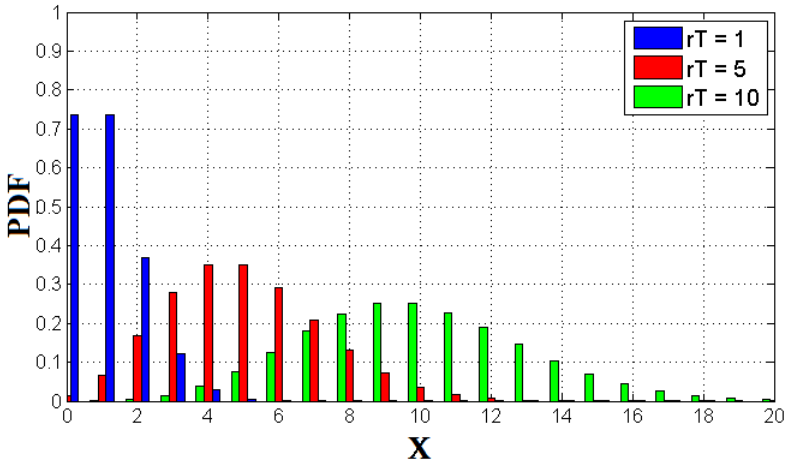

Figure 9: By increasing the rT as the probability of spikes occurring within a trial of duration T in Binomial equation, we can see the transition in the shape of probability of distribution function (PDF) from Poissonian to Gaussian.

5 Experimental Background

The dentate gyrus plays a major role at the entrance of hippocampus and acts as a filter, which converts the dense incoming information from the upstream entorthinal cortex into a sparse and distinct code indispensable for the formation and the discrimination of memory items [9].

Crépel et al. have reported that a new phenomenon corresponding to neuronal tissue alteration occurs in hippocampus, called reactive plasticity [8]. In reactive plasticity, some neurons die and some other which are more persistent, lead to sprouting of mossy fibers (granule cells axons) and generation of novel recurrent connections among granule cells (GCs), called recurrent mossy fiber (rMF). The rMF has been proposed to be at the base of epileptiform activities in the hippocampus. These activities or better known as seizure generation refers to an abnormal, excessive, and synchronized firing of a group of neurons.

In general, three main types of ionotropic receptors which are AMPA receptors (AMPAR), NMDA receptors (NMDAR), and Kainate receptors (KAR) are responsible for the glutamatergic excitatory drive which may contribute to seizure generation [17].

The KAR-operated synapses play a more important role in glutamatergic transmission, since $\mathrm{EPSC_{KA}}$ provides as much as half of the total spontaneous synaptic glutamatergic currents. Furthermore, these currents are originated from rMF synapses which operate via KAR, because by blockade of KAR significantly activities of mossy fiber network will decrease [17]. To explain in more details, in control DGCs, just fast AMPA receptor-mediated synaptic currents exists, while in epileptic DGCs, besides fast $\mathrm{EPSC_{AMPA}}$, long-lasting kainate receptor-mediated synaptic currents, or equivalently slow $\mathrm{EPSC_{KA}}$ also exist Fig. 10.

In the following subsections the experimental results when the system is under stimulation by external current will be discussed.

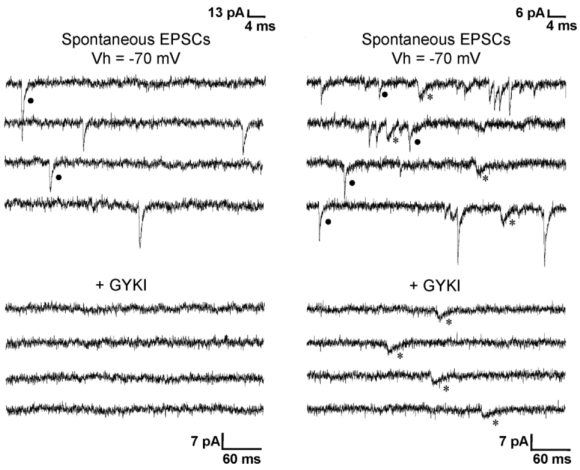

Figure 10: In healthy DGCs all the synaptic events are fast and mediated by AMPAR (upper left), since by blocking the AMPAR with GYKI (bottom left) there is no evidence of fast EPSC. However, in epileptic DGCs besides fast currents, slow synaptic events exist which are mediated by KAR (upper right), since in presence of GYKI just slow EPSC exists.

5.1 Single-Spike Stimulation

As I mentioned before, Kainate receptors have slower kinetic in comparison with AMPA receptors [18]. This difference in their kinetics will influence the spike timing precision during single spike stimulation experiment.

The precision of spike-time responses with different types of receptors was assessed by setting the membrane potential in a value such that a single EPSP would evoke 50% of the times an action potential (holding potential). The spike precision was estimated by calculating the latency between the onset of the EPSP and the emission of the spike, and standard deviation of the latencies [18].

During single kick stimulation, EPSPs evoked in healthy DGCs generated time-locked spikes at short latencies, while in epileptic DGCs the spikes occurred with different latencies, so in contrast to regular behaviour from healthy rats, irregular and jittered behaviour was observed from epileptic rats. The time-locked spiking is due to $EPSP_{fast}$ from AMPAR since they are only determinant parameters in healthy DGCs, while spikes with high temporal variability are caused by $EPSP_{slow}$ generating from KAR. It worth mentioning the action potential threshold, EPSP amplitude, half width and firing probability were not significantly different in healthy and epileptic DGCs, see Fig. 11.

Crépel et al. have reported that $EPSP_{KA}$ in DGCs from epileptic rats showed a strong voltage-dependent amplification which is mediated by the persistent sodium current (I_{NaP}). This current is activated below firing threshold and amplifies EPSPs in hippocampal and neocortical neurons. In contrast, $EPSP_{AMPA}$ recorded in DGCs from both control and epileptic rats were not significantly amplified with voltage.

As we can see in Fig. 12, the interplay between Kainate receptor and I_{NaP} results in amplification(upper left figure) with depolarization from -70mV to -50mV (upper right figure), while in the presence of Tetrodoxin (I_{NaP} blocker), we can see less irregular spiking in comparison with amplified case (bottom left). Thus, $EPSP_{KA}$ is selectively amplified with depolarization via the activation of I_{NaP} and this dramatically decreases the temporal precision of EPSP-spike coupling in DGCs from epileptic rats. As we mentioned before, I_{NaP} is a sodium current that activates below spike threshold and slowly inactivates. The slow kinetics of $EPSP_{KA}$ is sufficient to activate it and as a result, decreasing more the temporal precision.

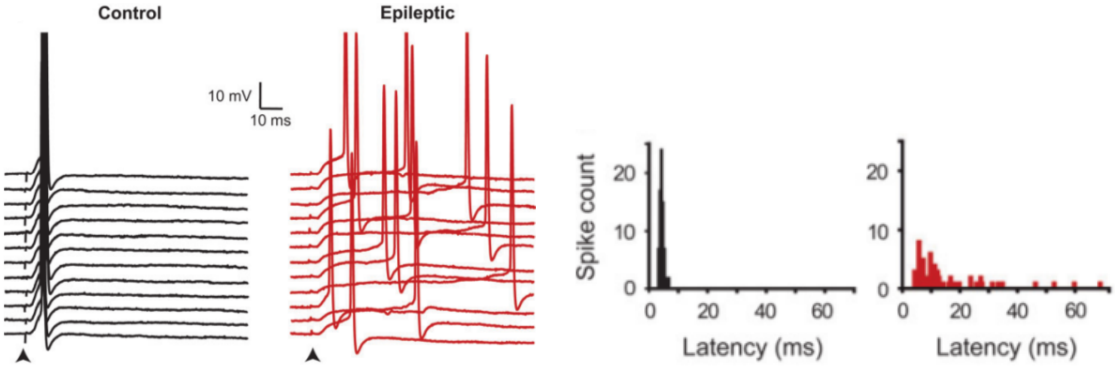

Figure 11: Latencies and corresponding histograms of healthy and epileptic rats after single spike stimulation. From healthy DGCs (black) the spiking is regular and distribution of latencies in the histogram is time-locked, while in epileptic DGCs (red) spikes occur irregularly and we can see the effect of this jittered behaviour in related histogram. This contrary behaviour is due to the kinetics of AMPAR and KAR.

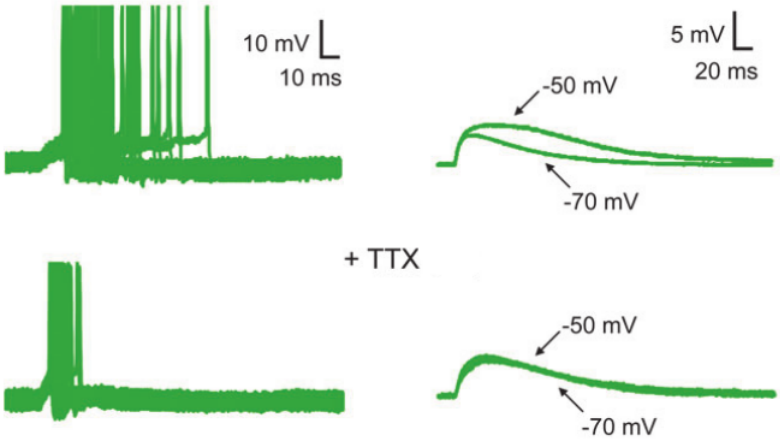

Figure 12: The Kainate receptor in interplay with I_{NaP} amplifies the jittered behaviour. By blocking the I_{NaP} with TTX (bottom left) we will have more regular spiking in comparison with the interplay case (upper left).

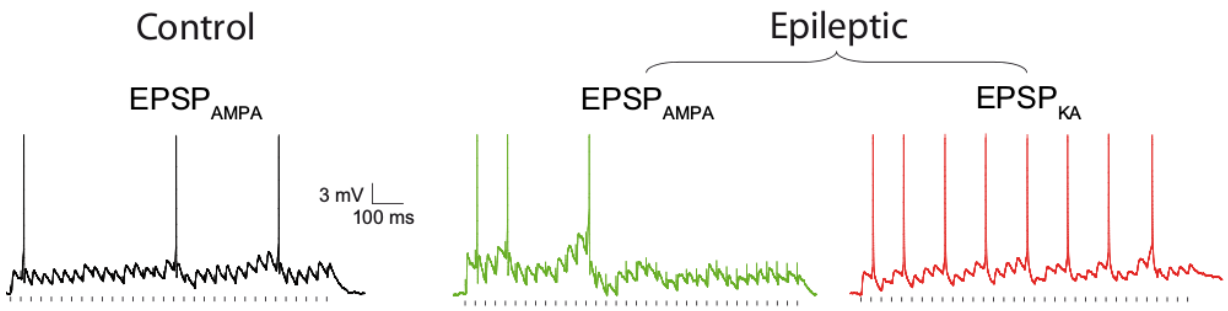

Figure 13: When the neuron is under periodic input injection, the EPSPs from AMPAR in both healthy and epileptic rats are irregular, while the EPSPs from KAR exhibit more regular behaviour.

To summarize, the change in EPSP-spike latency from control to epileptic rat is due to the slow kinetics of $EPSP_{KA}$ when compared with $EPSP_{AMPA}$, and not to intrinsic membrane properties or difference in EPSP amplitude. In addition, the slow shape of $EPSP_{KA}$ leads to activation of I_{NaP} which will amplify the jittered spikes and decrease the temporal precision.

5.2 Periodic-Spikes Stimulation

In this experiment [8], the neuron is stimulated with EPSPs generated periodically with a period T and a jitter from 10% to 100%.

In healthy rats, $EPSP_{AMPA}$ was recorded in the absence of KAR antagonist, because there is no rMF or reactive plasticity, but in epileptic rats, the data is obtained in the presence of AMPA and KA antagonist separately, so no interplay between $EPSP_{AMPA}$ and $EPSP_{KA}$ can be assessed.

Under various frequencies of stimulation , the trains of $EPSP_{AMPA}$ lead to a sparse firing regime for both healthy and epileptic rat, while in epileptic rat $EPSP_{KA}$ triggered sustained and rhythmic spikes, which is in contrast to previous result of single-spike stimulation. This paradoxical behaviour is just due to the difference in kinetics of AMPA and KA receptors, as shown in Fig. 13.

All in all, one of the possible interpretation of these data is that the slower kinetics of $EPSP_{KA}$ allows a high temporal summation, which in turn offsets the short-term depression, contrary to fast $EPSP_{AMPA}$. Since $EPSP_{KA}$ are periodic and more regular in comparison with $EPSP_{AMPA}$, the coefficient of variation (CV) of inter spike interval (ISI) for $EPSP_{KA}$ was dramatically lower than $EPSP_{AMPA}$ for different frequency of stimulation, as shown in Fig. 14.

As we reported earlier, the I_{NaP} strongly amplified $EPSP_{KA}$ at a sub-threshold potential in epileptic DGCs. Also in this experiment, the I_{NaP} is required to trigger the kainate receptor-driven rhythmic firing pattern. As a matter of fact, the role of I_{NaP} is in the regulation of excitability and rhythmic activity, because by blockade of I_{NaP} with tetrodoxin (TTX), the regularity of spiking from KAR was reduced and the CV was larger, in comparison with the case in which the TTX is absent, see Fig. 15. Thus, I_{NaP} plays a central role in the generation of the kainate receptor-driven firing pattern.

6 Results

We attempted to model the experimental set-up by considering a LIF neuron with and excitatory input that generates α-shaped synaptic response. Depending on the type of experiment (described in sections 5.1 and 5.2) a different type of input will be used. Since the main results rely on the differences of the kinetics of

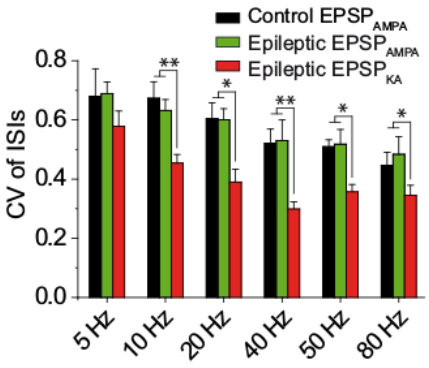

Figure 14: Since EPSPs generated from KAR are more regular, for different frequencies the CV of $\mathrm{EPSP_{KA}}$ is less than CV of $\mathrm{EPSP_{AMPA}}$.

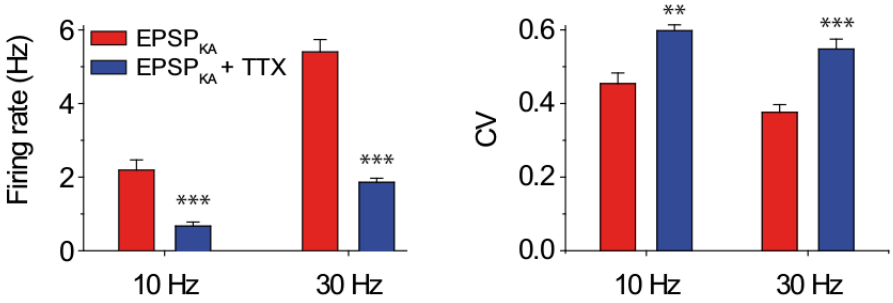

Figure 15: In the presence of TTX as $\mathrm{I_{NaP}}$ blocker, the CV of ISI form KAR is large. while in the absence of TTX the CV is reduced.

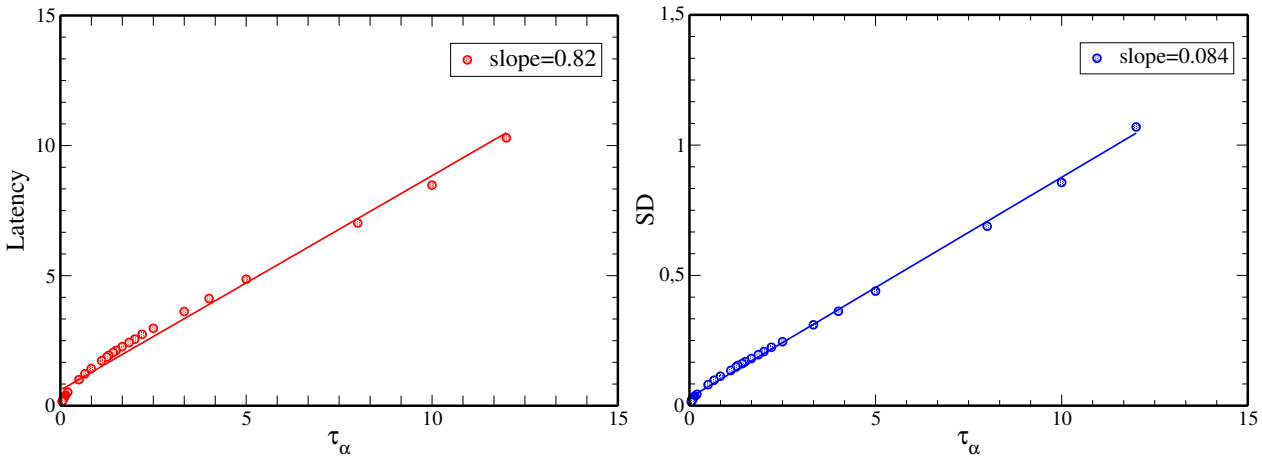

Figure 16: By increasing the decaying time of EPSP, the values of Latency (on the left) and its SD (on the right) will increase, which means the spiking time precision is decreasing and becoming more irregular. The membrane potential is set to a=0.66; each α has specific synaptic strength g, leading to generation of spikes in 50% of trials. The number of our trials was of the order of 10^4.

AMPA and Kainate receptors ($\text{EPSP}_{\text{fast}}$ and $\text{EPSP}_{\text{slow}}$ respectively), we will model these differences via the PSP time-scale parameter α [18].

6.1 Single-Spike Stimulation

For the experiment described in sec. 5.1, we set the membrane potential of the LIF neuron to a value equivalent to the holding potential. A simple comparison between the reported data in [18], and the conversion to the adimensional units of the LIF model allowed to estimate the value of the parameter and set it to $a = 0.66$.

A single EPSP is generated with an average strength g and a small variability $\Delta g = 10\% g$. Very small kicks will ever generate a spike, while very large kicks will generate it 100% of the trials. Following the guidelines described in [18], we will compare the values of g that generate spikes 50% of the trials for different values of the PSP time scale τ_α.

Once we have found the duplet [g, α] generating spikes 50% of the trials, we calculate in the spike generating trials, the average and standard deviation of the latency in the response. Results in this regard can be seen in Fig. 16. Both the average and the standard deviation of the latency increased by increasing the value of τ_α, which is in accordance with the experiment. For large τ_α which corresponds to KAR, the precision in the latency is reduced and the spikes were generated irregularly.

The number of our trials was of the order of 10^4, and the slopes of curves were obtained by linear fitting and its correlation coefficient was equal to 0.99.

6.2 Periodic-Spikes Stimulation

For the second experiment, we fix again the membrane potential (equivalently the a-value) to the holding potential as reported in [8]. To account for the periodic input we generate fixed-strength EPSPs periodically with a period T and a variability jitter (J), ΔT = J*T, and calculate the ISI statistics during the emission of 10^4 spikes. According to what reported in [8], by increasing input frequencies of stimulation ($\nu_i = 1/T$), the AMPA mediated activity produces a train of spikes with smaller precision than the Kainate mediated

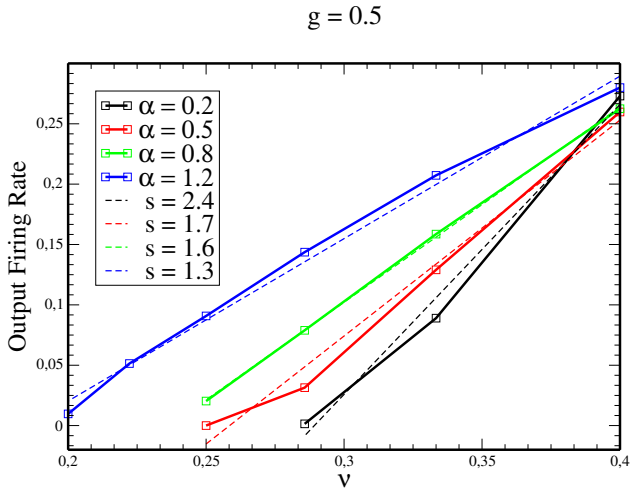

Figure 17: For $g = 0.5$ by increasing input frequency (ν) , the firing rate will increase. As we can see for frequencies larger than $\nu = 0.40$ there is a convergence in behaviour of the system for different EPSP. s indicates the value of slope for each curve which obtained with linear fitting and correlation coefficient equal to 0.98. The number of trials for obtaining data was of the order of 10^4.

activity. To estimate the values of g, α_{KA} and α_{AMPA} that better fit the experimental results, we examined a wide range of values for the parameters which reads as:

$$a = 0.83 \qquad \alpha \in [0.1, 5] \qquad g \in [0.1, 1] \qquad \nu \in [0.18, 0.80] \tag{32}$$

For each g, and different alpha, we calculate the "Response curve" (Output Firing Rate/Input Frequency) slope and the ratio between the slopes for all the possible pairs of alpha; the slopes of curves were obtained by linear fitting and its correlation coefficient was equal to 0.99.

We select the values g, α_{KA} and α_{AMPA}, as the closest-to-the-experimental value of the ratio between the slopes (see Fig. 17). These values are reported here:

$$g = 0.5 \qquad \alpha_{\text{KA}} = 0.2 \qquad \alpha_{\text{AMPA}} = 1.2 \tag{33}$$

For small values of g, we did not obtain results since the strength was too weak, also for too large values the firing rate was almost equal to input frequency ν. By increasing α, the slopes of the curves decrease, thus the maximum ratio of the slopes will be for $\alpha = 0.2$ and $\alpha = 1.2$, which we considered as Kainate and AMPA EPSP respectively. The reason why we did not consider larger value for α is that, since the pulses are too fast, we could not observe specific difference in behaviour of the system for α between 1.2 and 5. The other point is that for larger values of ν from 0.40 to 0.80 for different α, the behaviour of the systems did not change and curves were parallel, that's why in order to better demonstrate the effect of transition form small α to larger α, the results were illustrated until $\nu = 0.40$.

As a final issue, we plotted the ISI and CV of different α from 0.2 to 1.5 for different range of frequencies from 0.28 to 0.80. In each simulation we considered different percentage of jitter for the period of stimulation ($T = \frac{1}{\nu}$). In Fig. 18 we illustrated the behaviour of the system under 50% and 100% jitter:

From the experiment [8], we expected when the neuron is under periodic stimulation, the spikes from KAR be more regular than AMPAR. In other words, the CV of ISI for small α ($\text{EPSP}_{\text{fast}}$) be smaller than larger α ($\text{EPSP}_{\text{slow}}$). We obtained the same results for fast frequencies from 0.80 to almost 0.50, but for

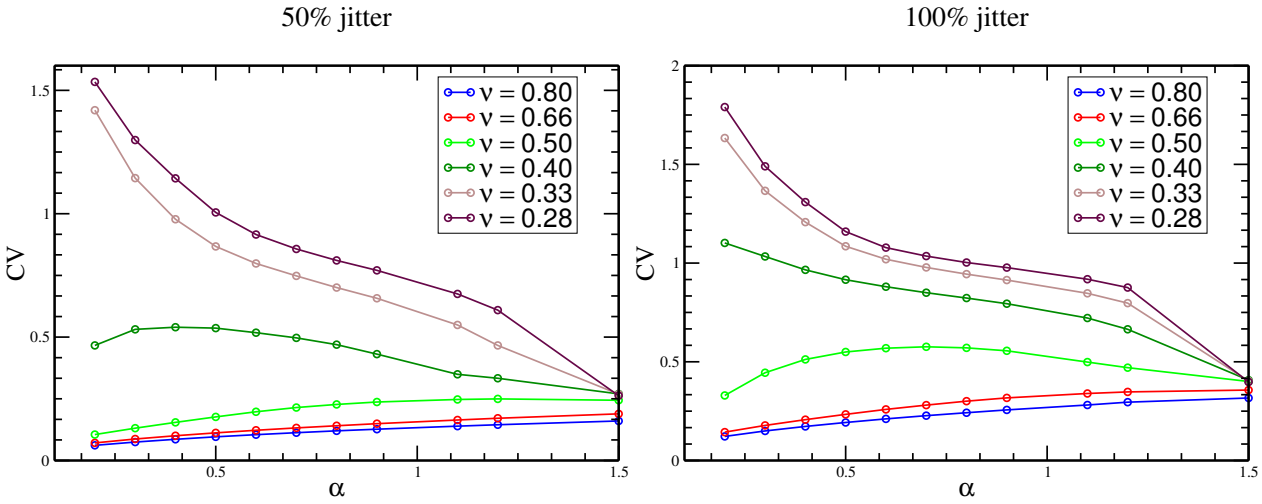

Figure 18: The contrasting behaviour in spikes regularity for $\text{EPSP}_{\text{slow}}$ by increasing the frequency of stimulation. By considering smaller values for jitter of period of stimulation, the jump will occur for smaller frequencies. The holding potential was set to a=0.83 equivalent to reported value in the experiment; the synaptic strength was equal g=0.5; The number of our trials for obtaining data and integration time for measuring CV was of the order of 10^4.

smaller frequencies we obtained contrary results. For small α (larger τ_α) the CV was larger, which indicates under periodic stimulation the spikes from KAR are more irregular than AMPAR.

For instance, in Fig. 19 we demonstrated the distribution of ISI for $\nu = 0.28$ for different α. In the left figure which $y - axis$ is in logarithmic scale, we can see for small α, the slope of distribution is lower which indicates the spiking occurs irregularly. For fast frequencies, since the synapse receives more stimulation during each PSP, the spiking occurs regularly, that's why the shape of its distribution is Gaussian (see Fig. 20), while in the previous case, the shape was Poissonian.

7 Conclusion

In this document we have briefly reviewed a new phenomenon described at the Hippocampus in epileptic rats, termed reactive plasticity. Reactive plasticity leads to the sprout of Mossy Fibers in the dentate gyrus producing aberrant recurrent excitatory connections. In particular we focused on the experimental results reported in [18], [8]. On one hand, in [18], it was demonstrated that under single EPSP stimulation of Granule Cells of healthy mice (AMPA mediated), the response of the neuron occurs via precise spike-timing with a fixed latency and small variability. In contrast, single EPSP stimulation of epileptic mice (Kainate mediated) produced a decrease in the spike-time precision, and therefore large variability in the latency of response. On the other hand, for a stimulation protocol consisting of periodic trains of EPSPs, granule cells of epilleptic mice emitted spikes at high frequency and low variability; this is in contrast to healthy mice that produced a sparse firing with high variability in the ISI.

By means of a simple model of a LIF neuron, receiving α-pulses, we aimed to emulate at qualitative extent some of the findings reported in the above mentioned experiments. The qualitative difference between epileptic and healthy cases was modelled through different time-scales of the incoming EPSP. AMPA mediated EPSP were assigned smaller time scales while Kainate EPSP were modelled through larger values of the time scale; this in accordance to the reported experimental results.

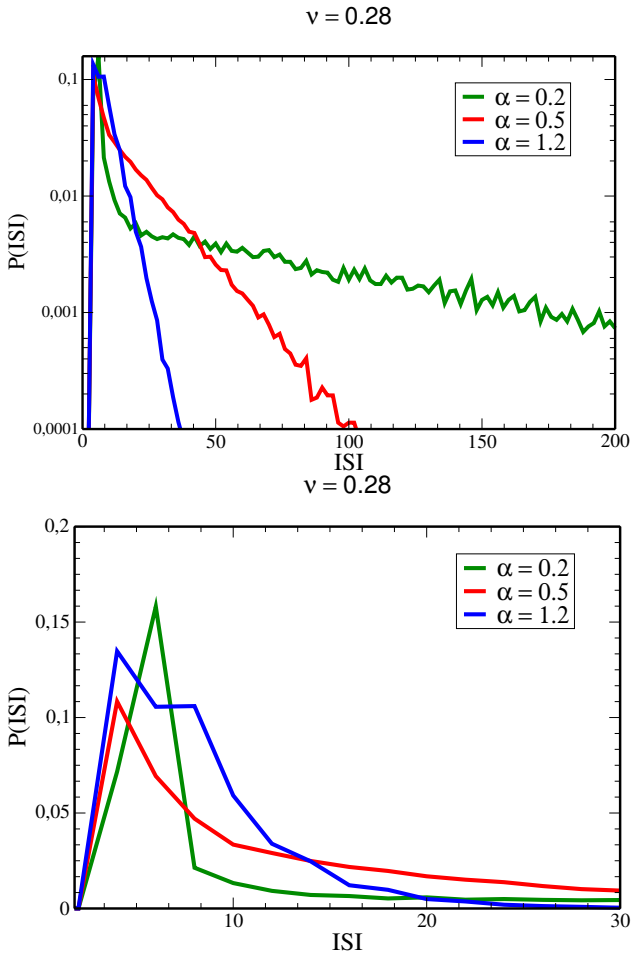

Figure 19: The distribution of inter-spike interval for $\nu = 0.28$. Since the frequency of stimulation is small, the shape of distribution is Poissonian and for $\alpha = 0.2$ its slope is smaller, which indicates the neuron fires more imprecise. In upper plot which the distribution is in Logarithmic scale we can compare the distribution of ISI for different α conveniently.

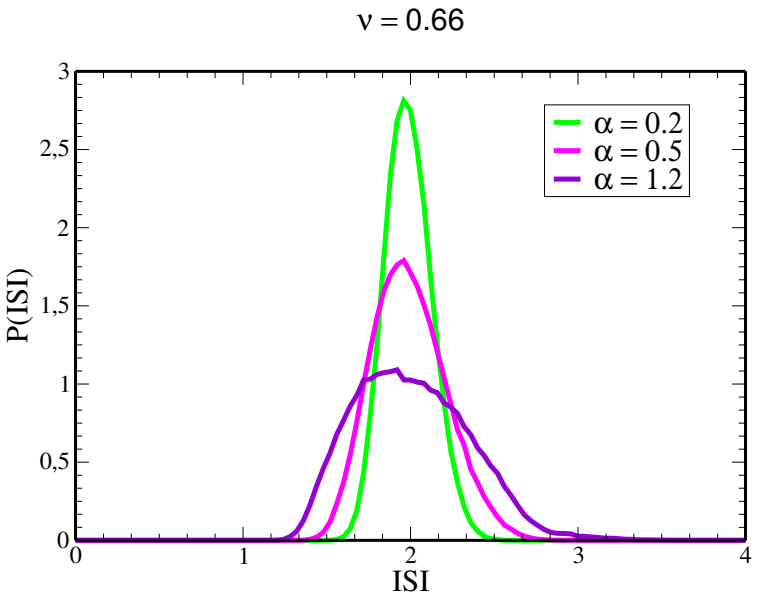

Figure 20: The distribution of inter-spike interval for $\nu = 0.66$. Since the frequency of stimulation is fast in respect to characteristic time scale of α-function, the neuron fired regularly and its shape of distribution is Gaussian. For small α which corresponds to large τ_α, the spikes occurred more precise and almost with same values, that's why the peak of distribution for $\alpha = 0.2$ is higher than other cases.

In the single EPSP stimulation protocol we found that the both the average and standard deviation of the latency between the EPSP onset and the spike emission grew with the time scale of the synapse. This results were in accordance with the experiment, where epileptic mice showed a reduced precision in the latency.

In contrast, for the periodic train of stimulation, we found that under certain range of stimulation frequencies, the "Response curve" behaves as expected from the experimental results, i.e, the slope of the curve is larger for slower synapses. Nevertheless, we saw that the variability of the ISI can increase or decrease with α depending on the stimulation frequency, contrary to what reported in [8]. We believe that the differences between the experiments and the model can be ascribed to the simplified nature of the LIF neuron, which is unable to capture several non-linear features of the original system.

In particular [36], has demonstrated that persistent sodium currents, which are voltage dependent can dramatically alter cell firing and facilitate hyperexcitability, since it will amplify their responses to synaptic inputs, thereby driving them to repetitive firing. It is worth to mention that the LIF does not consider any voltage dependent conductances and therefore we are not able to model these currents. Despite the simplicity of the LIF we were able to provide some insights in the generation of epileptiform activity in hippocamus, and we believe that future research with more complete models may provide useful explanations on novel phenomena during reactive plasticity.

Acknowledgements. We would like to show our gratitude to the group of Jérôme Epsztein and special thanks are due to Valérie Crépel, whom I will always be grateful for her encouragement of this project.
I also wish to acknowledge the generous support of our research by INMED-INSERM.

References

[1] LF Abbott and Carl van Vreeswijk. Asynchronous states in networks of pulse-coupled oscillators. *Physical Review E*, 48(2):1483, 1993.

[2] RW Aldrich, DP Corey, and CF Stevens. A reinterpretation of mammalian sodium channel gating based on single channel recording. *Nature*, 306(5942):436–441, 1983.

[3] Christian Alzheimer, Peter C Schwindt, and WE Crill. Modal gating of na+ channels as a mechanism of persistent na+ current in pyramidal neurons from rat and cat sensorimotor cortex. *The Journal of neuroscience*, 13(2):660–673, 1993.

[4] Per Andersen, Richard Morris, David Amaral, Tim Bliss, and John OKeefe. *The hippocampus book*. Oxford University Press, 2006.

[5] David Angulo-Garcia, Joshua D Berke, and Alessandro Torcini. Cell assembly dynamics of sparsely-connected inhibitory networks: a simple model for the collective activity of striatal projection neurons. *arXiv preprint arXiv:1511.06920*, 2015.

[6] David Angulo-Garcia and Alessandro Torcini. Stable chaos in fluctuation driven neural circuits. *Chaos, Solitons & Fractals*, 69:233–245, 2014.

[7] Alexander Arenz, Edward F Bracey, and Troy W Margrie. Sensory representations in cerebellar granule cells. *Current opinion in neurobiology*, 19(4):445–451, 2009.

[8] Julien Artinian, Angélique Peret, Geoffrey Marti, Jérôme Epsztein, and Valérie Crépel. Synaptic kainate receptors in interplay with inap shift the sparse firing of dentate granule cells to a sustained rhythmic mode in temporal lobe epilepsy. *The Journal of Neuroscience*, 31(30):10811–10818, 2011.

[9] Julien Artinian, Angélique Peret, Yanina Mircheva, Geoffrey Marti, and Valérie Crépel. Impaired neuronal operation through aberrant intrinsic plasticity in epilepsy. *Annals of neurology*, 77(4):592–606, 2015.

[10] Romain Brette. Exact simulation of integrate-and-fire models with synaptic conductances. *Neural Computation*, 18(8):2004–2027, 2006.

[11] Peter R Brink, Kerry Cronin, and SV Ramanan. Gap junctions in excitable cells. *Journal of bioenergetics and biomembranes*, 28(4):351–358, 1996.

[12] Anthony N Burkitt. A review of the integrate-and-fire neuron model: I. homogeneous synaptic input. *Biological cybernetics*, 95(1):1–19, 2006.

[13] Michael A Colicos and Pramod K Dash. Apoptotic morphology of dentate gyrus granule cells following experimental cortical impact injury in rats: possible role in spatial memory deficits. *Brain research*, 739(1):120–131, 1996.

[14] Wayne E Crill. Persistent sodium current in mammalian central neurons. *Annual Review of Physiology*, 58(1):349–362, 1996.

[15] Peter Dayan and Laurence F Abbott. *Theoretical neuroscience*, volume 806. Cambridge, MA: MIT Press, 2001.

[16] Niels Eijkelkamp, John E Linley, Mark D Baker, Michael S Minett, Roman Cregg, Robert Werdehausen, François Rugiero, and John N Wood. Neurological perspectives on voltage-gated sodium channels. *Brain*, 135(9):2585–2612, 2012.

[17] Jérôme Epsztein, Alfonso Represa, Isabel Jorquera, Yehezkel Ben-Ari, and Valérie Crépel. Recurrent mossy fibers establish aberrant kainate receptor-operated synapses on granule cells from epileptic rats. *The Journal of neuroscience*, 25(36):8229–8239, 2005.

[18] Jérôme Epsztein, Elisabetta Sola, Alfonso Represa, Yehezkel Ben-Ari, and Valérie Crépel. A selective interplay between aberrant epspka and inap reduces spike timing precision in dentate granule cells of epileptic rats. *Cerebral Cortex*, page bhp156, 2009.

[19] CR French, P Sah, KJ Buckett, and PW Gage. A voltage-dependent persistent sodium current in mammalian hippocampal neurons. *The Journal of General Physiology*, 95(6):1139–1157, 1990.

[20] Wulfram Gerstner, Werner M Kistler, Richard Naud, and Liam Paninski. *Neuronal dynamics: From single neurons to networks and models of cognition*. Cambridge University Press, 2014.

[21] Wm F Gilly and Clay M Armstrong. Threshold channels–a novel type of sodium channel in squid giant axon. *Nature*, 309(5967):448–450, 1983.

[22] Alan L Goldin. Mechanisms of sodium channel inactivation. *Current opinion in neurobiology*, 13(3):284–290, 2003.

[23] Alan L Hodgkin and Andrew F Huxley. A quantitative description of membrane current and its application to conduction and excitation in nerve. *The Journal of physiology*, 117(4):500, 1952.

[24] Sheriar G Hormuzdi, Mikhail A Filippov, Georgia Mitropoulou, Hannah Monyer, and Roberto Bruzzone. Electrical synapses: a dynamic signaling system that shapes the activity of neuronal networks. *Biochimica et Biophysica Acta (BBA)-Biomembranes*, 1662(1):113–137, 2004.

[25] JR Hotson, DA Prince, and PA Schwartzkroin. Anomalous inward rectification in hippocampal neurons. *Journal of Neurophysiology*, 42(3):889–895, 1979.

[26] Eugene M Izhikevich. *Dynamical systems in neuroscience*. MIT press, 2007.

[27] Eric R Kandel, James H Schwartz, Thomas M Jessell, et al. *Principles of neural science*, volume 4. McGraw-hill New York, 2000.

[28] JA Kearney, NW Plummer, MR Smith, J Kapur, TR Cummins, SG Waxman, AL Goldin, and MH Meisler. A gain-of-function mutation in the sodium channel gene scn2a results in seizures and behavioral abnormalities. *Neuroscience*, 102(2):307–317, 2001.

[29] Massimo Mantegazza, Giulia Curia, Giuseppe Biagini, David S Ragsdale, and Massimo Avoli. Voltage-gated sodium channels as therapeutic targets in epilepsy and other neurological disorders. *The Lancet Neurology*, 9(4):413–424, 2010.

[30] Toshiaki Nakashiba, Jesse D Cushman, Kenneth A Pelkey, Sophie Renaudineau, Derek L Buhl, Thomas J McHugh, Vanessa Rodriguez Barrera, Ramesh Chittajallu, Keisuke S Iwamoto, Chris J McBain, et al. Young dentate granule cells mediate pattern separation, whereas old granule cells facilitate pattern completion. *Cell*, 149(1):188–201, 2012.

[31] D. Purves. *Neuroscience*. Sinauer Associates, 2012.

[32] Wilfrid Rall. Distinguishing theoretical synaptic poten-tials computed for different soma-den-dritic distributions of synaptic input. 1967.

[33] DAVID A Saint, YK Ju, and PETER W Gage. A persistent sodium current in rat ventricular myocytes. *The Journal of Physiology*, 453:219, 1992.

[34] PETER C Schwindt and WAYNE E Crill. Amplification of synaptic current by persistent sodium conductance in apical dendrite of neocortical neurons. *Journal of Neurophysiology*, 74(5):2220–2224, 1995.

[35] Larry Squire, Darwin Berg, Floyd E Bloom, Sascha Du Lac, Anirvan Ghosh, and Nicholas C Spitzer. *Fundamental neuroscience*. Academic Press, 2012.

[36] Carl E Stafstrom. Persistent sodium current and its role in epilepsy. *Epilepsy Currents*, 7(1):15–22, 2007.

[37] David Sterratt, Bruce Graham, Andrew Gillies, and David Willshaw. *Principles of computational modelling in neuroscience*. Cambridge University Press, 2011.

[38] Gaia Tavosanis. Dendritic structural plasticity. *Developmental neurobiology*, 72(1):73–86, 2012.

[39] Charles P Taylor. Na+ currents that fail to inactivate. *Trends in neurosciences*, 16(11):455–460, 1993.

[40] Thomas Trappenberg. *Fundamentals of computational neuroscience*. OUP Oxford, 2009.

[41] Cuiyong Yue, Stefan Remy, Hailing Su, Heinz Beck, and Yoel Yaari. Proximal persistent na+ channels drive spike afterdepolarizations and associated bursting in adult ca1 pyramidal cells. *The Journal of neuroscience*, 25(42):9704–9720, 2005.

[42] Rüdiger Zillmer, Roberto Livi, Antonio Politi, and Alessandro Torcini. Stability of the splay state in pulse-coupled networks. *Physical Review E*, 76(4):046102, 2007.